**Amin A.M. Fadlalla**
Assistant Professor
Mechatronics Engineering Department
Faculty of Engineering
Mashreq University
Sudan

**Ahmet Z. Sahin**
Professor
Aeronautical Engineering Department
Faculty of Aeronautics and Astronautics
Istanbul Technical University
Maslak 34469, Istanbul
Turkey

**Hassen M. Ouakad**
Associate Professor
Mechanical & Industrial Engineering Department
Faculty of Engineering
Sultan Qaboos University
Oman

**Haitham Bahaidarah**
Professor
Mechanical Engineering Department
King Fahd University of Petroleum & Minerals
Faculty of Engineering
Saudi Arabia

# Aeroelastic Analysis of Straight-bladed Vertical Axis Wind Turbine Blade

*To prevent flutter phenomena in a wind turbine, minimize vibration and increase the blades' life, a systematic analysis is required to investigate the effects between the cyclic aerodynamic loads and the structural performance of the turbine. A dynamic analysis of a straight-bladed vertical axis wind turbine (SB-VAWT) blade is investigated in this paper, and a simplified approach for the energy equations of an Eulerian beam subjected to twist and transverse bending deflections is introduced. The aerodynamic loads are estimated using the double multiple stream tube models. They are introduced into the dynamic model in the aeroelastic coupling, where the structural displacements are fed back to update the aerodynamic loads by utilizing the average acceleration method for the numerical integration of the equations. Reduced order modeling is then imposed based on the first modes of vibration. It is found that the structural displacement has little effect on the aerodynamic loads, and SB-VAWTs experience higher transverse displacements compared with those in curved-blade VAWTs.*

***Keywords:*** *aeroelastic structural analysis, straight bladed VAWTs, thin beam theory, reduced order modeling, DMST model*

## 1. INTRODUCTION

Several researchers have addressed various aspects of the aeroelastic analysis and dynamic modeling of VAWTs. A simplified analytical model of an SB-VAWT is introduced in [1] to study and analyze the dynamics of the supporting masts, considering the mix between the mast and the rotor. It is found that the two leading dynamic issues in masts design are the extreme movement at the top of the tower and the fatigue of welded elements. Besides, many countries [2,3] have investigated wind energy potential and optimal locations of wind turbines.

The nonlinear, 2nd degree, aeroelastic equations for a slender, nonuniform, supple, Darrieus VAWT blade are withstanding amalgamated edgewise bending, flatwise bending, extension, and torsion, have been investigated in [4] utilizing the principles of Hamilton. The aerodynamic loads acting on the blade are found from strip theory grounded on a quasi-steady estimation of incompressible, two-dimensional, unsteady airfoil the–ory. The obtained equations derived based on the geometric-nonlinear theory of elasticity, are compatible with the small deformation estimation. The resulting equations were reported to be appropriate for examining the dynamic response, aeroelastic instabilities, and vibrations. Some potential approaches to solutions to the equations were suggested.

Nitzsche [5] distinctively derived a rigorous set of dynamic equations of motion of a curved-blade VAWT blade, which account for the Coriolis effect, centrifugal softening, and centrifugal stiffening. The equations were coupled with the quasi-steady aerodynamic loading to evaluate the aeroelastic instability of the VAWTs. Based on Theodorsen's theory, the aerodynamic loading does not consider the stall conditions, wake effect, and flow instability. In [6], the structural dynamic equations devised by Nitzsche [5] are cast into mixed finite element forms and coupled with the free vortex model. A package named FEM-Vort (aeroelastic analysis tool) is utilized to estimate the structural responses and aerodynamic execution of the DOE/Sandia 17m VAWT. The numerical results have been compared with the accessible experimental data, which showed an excellent agreement except where dynamic stall plays an important role.

The design and analysis of a small-scale SB-VAWT blade utilizing numerical and analytical techniques are presented in [7]. It is found that the centrifugal forces play a vital role and significantly affect both the bending stresses and deflections. In [8], the aerodynamics of the wavy blade under the effect of fluctuated wind flow is studied. It is found that the wavy blade can behave better in turbulent wind conditions with a maximum lift coefficient of 0.73 compared to 0.621 for the normal blade. On the other hand, wind turbine blades are increasingly changing in size and complexity, becoming larger and more complex, and their construction involves a comprehensive collection of materials and manufacturing techniques. The paper [9] harmonization of new wind turbine rotor blades development process is studied. It presents the har–monization of new wind turbine rotor blade deve–lopment and the analysis of behavior by verification testing for a wind turbine rotor blade of composite materials. Besides, the vital role of the blade develop–ment and design, the optimization in the operation of the entire wind turbine farm is of great importance, as detailed in [10]. An approach for determining optimum positions of single wind turbines within the wind farms

Received: February 2022, Accepted: July 2022
Correspondence to: Dr Ahmet Z. Sahin
Faculty of Aeronautics and Astronautics, Istanbul Technical University, Maslak 34469 Istanbul Turkey
E-mail: sahinaz@itu.edu.tr
**doi:10.5937/fme2203512F**

installed on arbitrarily configured terrains is presented to achieve their maximum production effectiveness. The genetic algorithm was used as the root optimization technique with two different fitness functions both involve the total energy obtained from the wind farm as one variable; other variables include the total inves–tment in a single turbine and the number of turbines. Other studies on the optimization of VAWTs blades and aerofoils are given in [11,12].

A vibration model for an SB-VAWT blade for twisting and bending deflections has been investigated in [13,14], where energy equations for the Euler-Bernoulli beam subjected to twist and transverse bending deviations have been introduced. Reduced order modeling was used to discretize the system based on foremost presumed modes on every independent variable in the equations. By applying the Lagrange approach to the obtained equations, two equations of motion were found where aeroelastic forces on the blades have been used as generalized forces. Based on the quasi-static airfoil theory, an aeroelastic model was then described. Moments and forces of lift and drag were formulated for an airfoil of varying attach angles, neglecting the stall effects. Taylor series expansion was utilized to simplify the obtained complex formulas to cubic order. Supposing that are small deflections for twist and bend, the system was linearized, and a simple numerical analysis was conducted. Obtained numerical results showed intricated dynamics and a tendency for instability.

In [15,16], a modal analysis of the Darrius VAWT blade having a troposkein geometry is introduced where the main objective was to find the modal frequencies and mode shapes of the blade's free vibration, where the change of the upstream wind speed was ignored to simplify the analysis. The blade model was investigated analytically where Euler-Bernoulli theory &the method of assumed modes were utilized numerically using ANSYS FEA software. Both ideal a troposkein and Sandia simplified troposkein-shaped blade have been considered, and comparable results were obtained. The blade vibration under flatwise, edgewise, torsional, and extensional deformations were studied, and the first ten modes have been identified for stationary and rotating blade conditions. Wind farm layout design was optimized using particle swarm optimization was examined in [17]. It is found that, the acceleration coefficients impact the final layout quality, leading to better overall energy output. Moreover, Honeycomb core composite plates are becoming more important in constructing primary aerospace structures such as wings and wind turbine blades [18].

The aeroelastic stability of the Darrieus VAWT has gained little recognition in the literature [19], mainly because it was not earnestly contemplated as an alternative to the more typical HAWT until the early 1970s. On the other hand, the HAWT is like a helicopter rotor and despite notable differences exist among them, the comprehensive research which has been performed on helicopter rotors over the past thirty years has yielded a solid base for the aeroelastic analysis of HAWTs. Regrettably, no such background exists for the Darrieus rotor. Thus, a more fundamental approach is needed. The study of such interactions between the unsteady aerodynamic forces and the elastic & inertia forces of the structure is called aeroelasticity. Under specific conditions, these forces can lead to unstable vibrations, a potentially critical problem known as flutter [20]. Other investigations involving wind turbine modeling and analysis are given in [21–23].

The main objective of this study is to investigate the aeroelastic analysis of SB-VAWTs blade, which has not been compressively discussed in the literature as most of the previous studies were related to CB-VAWTs and HAWTs. This aeroelastic analysis will help investigate the reciprocal effects of structural deformations such as bending & twisting and the aerodynamic performance of the turbine to reduce the vibration level and con–sequently increase the blade's life in the wind turbine system.

In the proposed approach, thin beam theory and reduced order modeling are used to formulate energy equations, then the Lagrange equation is employed to deduce the dynamic of the system, as detailed in section 2. As for the aerodynamic loads' estimation, DMST is utilized as given in section 3. After that, the aerody–namic loads are introduced to the dynamic model in the aeroelastic coupling, where the structural displacements are fed back to update the aerodynamic loads, which is the subject of the fourth section. Finally, in section 5, the main results are presented and discussed, followed by a conclusions section.

## 2. MODELING AND FORMULATION

The main component subjected to great deformation in the VAWT system is the blade which is handled as a straight uniform beam subjected to deformations of mainly twisting and bending. Energy equations deri–vation for the twisting and bending of the blade is introduced first, accompanied by a simplified aero–dynamics model based on momentum theory to find the moment, lift & drag forces expressions as functions of spatial position on the blade and time. Next, the aero–elastic coupling of the aerodynamic and structural dy–namic model is discussed.

Before proceeding, some assumptions were made:

1) Constant speed of the wind
2) Wind disturbance due to the tower or upstream blade is disregarded
3) Fixed rotation speed (RPM)
4) Unstretchable beam
5) Edgewise bending is negligible compared to flatwise bending
6) The Center of flexure (shear center)coincides with the blade’s geometric Center

The geometric center of the blade is the arithmetic mean position of all the points in the blade (i.e., the center point of the blade). If the blade has a uniform density, its geometric Center is the Center of mass. The last assumption is important since the bending and torsional vibrations will be uncoupled when the centroid and the shear center (Center of flexure) coincide [24].

Moreover, the aerofoil cross section has a major (chord-length) axis and a minor axis. Bending about the major axis is called "flat-wise," and bending about the

minor axis is regarded as "edgewise.". In other words, flatwise is the same as flap-wise, while edgewise is the in-plane vibration.

### 2.1 Elastic Blade Model for Bending

Transverse bending refers to blade deflection in the radial direction, while the twisting takes place about an axis that proceeds along the centroid of a blade cross-section. The blade under modeling may sustain bend-bend-twist swerving. However, only 1D transverse bending and twisting will be considered. Initially, energy equations for the beam particles will be exp–ressed to allow the application of Lagrange formulation based on assumed modes.

Thus, sections throughout the axis of the unde–formed blade (beam) will be positioned from an origin at the turbine mid-centre (as shown in Fig. 1) using the following position vector [13]:

$$r(x,t) = (x - s(x,t))\hat{i} + (R + y(x,t))\hat{e}_r \quad (1)$$

In (1), r and R are the radii of the deformed and undeformed rotor, respectively, x is the vertical position of the blade section with respect to the origin, $y(x,t)$ and represents the transversal displacement of the chosen blade section at time t in the radial direction, $s(x,t)$is the amassing foreshortening term influencing point x at time t because of deflection. For $x > 0$, this term is considered positive. Also, the unit vector $\hat{i}$ is along the undeformed x-axis and $\hat{e}_r$ is in y direction, radial to the Center of rotation, as shown in Fig. 2. The coordinate system x*yz* is attached at the Center of the rotor and rotating with it such that at any time $j=\hat{e}_r$ & $k = \hat{e}_\theta$.

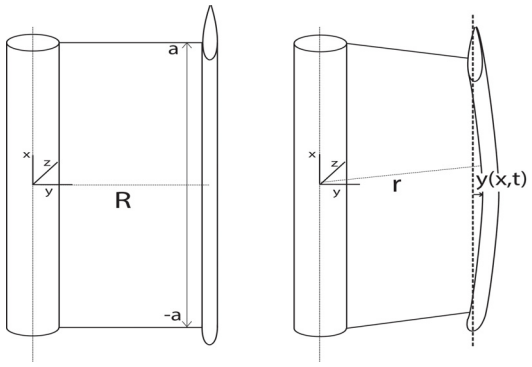


**Figure 1. A diagram of rotor and blade in the deformed and undeformed configuration**

The foreshortening term for an Euler-Bernoulli beam caused by 1Dtransverse bending in the outward (radial) direction y (retaining terms up to 4th degree) can be formulated as [14]:

$$s(x,t) \cong \int_{-a}^{+a}\left(\frac{y'^2}{2} + \frac{y'^4}{8}\right)dz \quad (2)$$

which will introduce first and third-order terms to the equations where *a* is the blade's half-length. Considering the fixed speed of rotation and ignoring the transverse deflection's effects on the peripheral side of the energy, the kinetic energy of the beam particles can be for–mulated as

$$T = \int_{-a}^{+a}\frac{1}{2}m(x)v^2(x,t)dx + \int_{-a}^{+a}\frac{1}{2}J_{xx}(\dot{\psi}+\Omega)^2dx + \frac{1}{2}I_0\dot{\theta}^2 \quad (1)$$

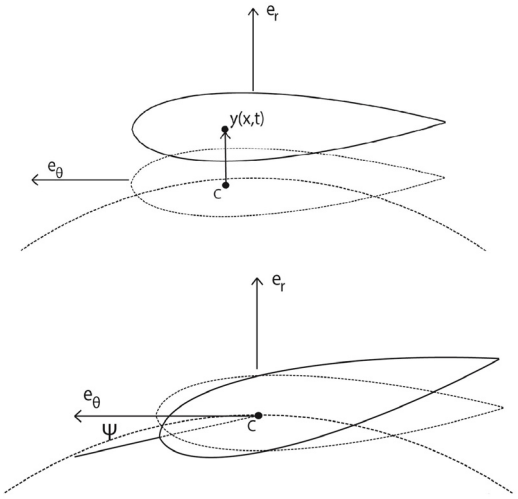


**Figure 2. Top view schematic of (a) the blade twist on the bottom and (b) transverse deflection at the top.**

where $I_0$ is the rotor mass moment of inertia, $\psi$ is the angle of twist deformation, $m(x)$ is the mass per unit length of the beam, and $J_{xx}$ is the second moment of the area around the centroid. In addition, v is the velocity which is the rate of change of the position vector $s(x,t)$, defined as

$$v = \dot{r} = -\dot{s}i + \dot{y}\hat{e}_r + \Omega\big(y(x,t) + R\big)k \quad (3)$$

where $\Omega = \dot{\theta}$ is the angular velocity of the rotating parts that is fixed.

Likewise, the potential energy will be developed in terms of integrations also. The whole potential energy V is expressed by summing the strain energy due to bending and twist, $V_s$, the elastic potential energy of the beam boundaries, $V_b$, and gravitational potential energy, $V_{mg}$.

Therefore, disregarding the blade's net vertical def–lections:

$$V_{mg} = \int_{-a}^{+a} m(x)\,g\big(x - s(x,t)\big)dx \quad (4)$$

$$V_s = \int_{-a}^{+a}\frac{1}{2}EI_{zz}(x)\Big[y''^2(1-3y'^2)\Big]dx + \int_{-a}^{+a}\frac{1}{2}GI_{xx}(x)\psi'^2dx \quad (5)$$

$$V_b = \frac{1}{2}k_1\big(-s(-a,t)\big)^2 + \frac{1}{2}k_{T_1}\big(y'(-a,t)\big)^2 + \frac{1}{2}k_2\big(-s(a,t)\big)^2 + \frac{1}{2}k_{T_2}\big(y'(a,t)\big)^2 \quad (6)$$

where E is the modulus of elasticity and $I_z(x)$ is the second moment of the area around the chord line, $I_{xx}(x)$ the mass moment of inertia around the cross-section of the blade about the centroid per unit length of the blade. $V_s$ Comprises nonlinear bending curvature effects estimated to the fourth degree. It is worth mentioning that the elastic modeling contains two parts per strut. The latter is considered as superposed torsional and linear springs having torsional spring constants as $k_{T_1}$ and $k_{T_2}$, and $k_1$ & $k_2$ as the linear constants for the first and second strut.

### 2.2 Reduced Order Modelling

Here we apply Lagrange's equation on assumed modal coordinates where beam deflections are projected on pinned-pinned beam modes to find nonlinear 2nd order ordinary differential equations. Considering formulation of an assumed mode [25]:

$$\tau_k(x,t) \approx \sum_{i=1}^{N} \zeta_i(t)\eta_i(x) \tag{7}$$

where N is the assumed modes number, $\tau$ the deflection, $\zeta_i(t)$ the assumed modal coordinates, and $\eta_i(x)$ the assumed modal functions. In the case of the SB-VAWT blade, where transverse deflection (y) and twist ($\psi$) are consi–dered, we can write (using one assumed mode for each):

$$\begin{aligned} &\mathrm{y}(x,t) \approx q(t)\zeta(x) \\ &\psi(x,t) \cong b(t)\rho(x) \end{aligned} \tag{8}$$

To find equations of motion, appropriate terms of (9) are introduced to energy equations (3-7) and substituting the result into Lagrange's equation:

$$\frac{\partial}{\partial t}\left(\frac{\partial T}{\partial \dot{q}_k}\right) - \frac{\partial T}{\partial q_k} + \frac{\partial V}{\partial q_k} = Q_k \tag{9}$$

where V is the potential energy, T is the kinetic energy, and the dependent variable $q_k$ is the generalized coordinate, k = 1, 2…. n. $Q_k$ is the term of the generalized force. The work of non-conservative forces is given by:

$$\delta W_{nc} = Q_q \delta q + Q_b \delta b \tag{10}$$

where

$$Q_q = \int_{-a}^{a} F_n \zeta(x)dx \qquad Q_q = \int_{-a}^{a} M\rho(x)dx \tag{11}$$

where $F_n$ s the aerodynamic force per unit length in the normal direction and $M$ is the aerodynamic moment per unit length. The obtained equations of motions for bending and twisting, respectively, are:

$$\begin{aligned} &q\dot{q}^2 \int_{-a}^{a} m(x)\left[\int_0^x (\zeta')^4 dz\right]dx + q^2\ddot{q}\int_{-a}^{a} m(x)\left[\int_0^x (\zeta')^4 dz\right]dx + \ddot{q}\int_{-a}^{a} m(x)\zeta^2 dx - q\int_{-a}^{a} m(x)\Omega^2\zeta^2\,\mathrm{dx} \\ &-q\int_{-a}^{a} gm(x)\left[\int_0^x (\zeta')^2 dz\right]dx - q^3\int_{-a}^{a} g\frac{m(x)}{2}\left[\int_0^x (\zeta')^4 dz\right]dx - \int_{-a}^{a} m(x)\Omega^2 R\zeta dx + q\int_{-a}^{a} EI_z(x)\zeta''^2 dx \\ &-q^3\int_{-a}^{a}\left[6EI_z(x)\zeta''^2\zeta'^2\right]dx + q\left(\mathrm{k}_{T_1}+k_{T_2}\right)\left(\zeta'|_{\pm a}\right)^2 + q^3\frac{k_1+k_2}{2}\left[\int_0^{\pm a}(\zeta')^4\left(1+\tfrac{1}{4}q^2\zeta'^2\right)\left(1+\tfrac{1}{2}q^2\zeta'^2\right)dx\right] \\ &+q^4\ddot{q}\int_{-a}^{a} m(x)\left[\int_0^x (\zeta')^6 dz\right]dx + 2q^3\dot{q}^2\int_{-a}^{a} m(x)\left[\int_0^x (\zeta')^6 dz\right]dx + \frac{1}{4}q^6\ddot{q}\int_{-a}^{a} m(x)\left[\int_0^x (\zeta')^8 dz\right]dx \\ &+\frac{3}{4}q^5\dot{q}^2\int_{-a}^{a} m(x)\left[\int_0^x (\zeta')^8 dz\right]dx = Q_q \end{aligned} \tag{12}$$

$$\ddot{b}\int_{-a}^{a} I_{xx}\rho^2 dx + b\int_{-a}^{a} GJ_{xx}\rho'^2 dx = Q_b \tag{13}$$

Neglecting the higher order terms (more the 4th order), the obtained equations of motion are:

$$\begin{aligned} &q\dot{q}^2 \int_{-a}^{a} m(x)\left[\int_0^x (\zeta')^4 dz\right]dx + q^2\ddot{q}\int_{-a}^{a} m(x)\left[\int_0^x (\zeta')^4 dz\right]dx + \ddot{q}\int_{-a}^{a} m(x)\zeta^2 dx - q\int_{-a}^{a} m(x)\Omega^2\zeta^2\,\mathrm{dx} \\ &-q\int_{-a}^{a} gm(x)\left[\int_0^x (\zeta')^2 dz\right]dx - q^3\int_{-a}^{a} g\frac{m(x)}{2}\left[\int_0^x (\zeta')^4 dz\right]dx - \int_{-a}^{a} m(x)\Omega^2 R\zeta dx + q\int_{-a}^{a} EI_z(x)\zeta''^2 dx \\ &-q^3\int_{-a}^{a}\left[6EI_z(x)\zeta''^2\zeta'^2\right]dx + q\left(\mathrm{k}_{T_1}+k_{T_2}\right)\left(\zeta'|_{\pm a}\right)^2 + q^3\frac{k_1+k_2}{2}\left[\int_0^{\pm a}(\zeta')^4\left(1+\tfrac{1}{4}q^2\zeta'^2\right)\left(1+\tfrac{1}{2}q^2\zeta'^2\right)dx\right] = Q_q \end{aligned} \tag{14}$$

$$\ddot{b}\int_{-a}^{a} I_{xx}\rho^2 dx + b\int_{-a}^{a} GJ_{xx}\rho'^2 dx = Q_b \tag{15}$$

where $Q_q$ and $Q_b$ are non-conservative aerodynamic forces to be formulated.

### 2.3 Linearization

To simplify the analysis, a linearized model of the system is to be determined. The linearization is per–formed at the equilibrium position of a stationary rotor.

Hence, the linear model is found by supposing ψ and y are small. Therefore, second and third order terms in b & q and their rates are neglected. Thus, considering small deflections, the resulting equations for the case of single assumed mode are given as:

$$\begin{aligned} &\ddot{q}\int_{-a}^{a} m(x)\zeta^2 dx - q\int_{-a}^{a} m(x)\Omega^2\zeta^2\,\mathrm{dx} - q\int_{-a}^{a} gm(x)\left[\int_0^x (\zeta')^2 dz\right]dx \\ &-\int_{-a}^{a} m(x)\Omega^2 R\zeta dx + q\int_{-a}^{a} EI_z(x)\zeta''^2 dx + q\left(\mathrm{k}_{T_1}+k_{T_2}\right)\left(\zeta'|_{\pm a}\right)^2 = Q_q \end{aligned} \tag{16}$$

$$\ddot{b}\int_{-a}^{a} I_{xx}\rho^2 dx + b\int_{-a}^{a} GJ_{xx}\rho'^2 dx = Q_b \tag{17}$$

In matrix form, the linearized equations (17-18) will be written as:

$$\begin{bmatrix} m_{11} & m_{12} \\ m_{21} & m_{22} \end{bmatrix}\begin{bmatrix} \ddot{q} \\ \ddot{b} \end{bmatrix} + \begin{bmatrix} k_{11} & k_{12} \\ k_{21} & k_{22} \end{bmatrix}\begin{bmatrix} q \\ b \end{bmatrix} = \begin{bmatrix} Q_q^* \\ Q_b \end{bmatrix} \tag{18}$$

Where the elements of the mass and stiffness matrices are written as:

$$\bar{M} = \begin{bmatrix} m_{11} & m_{12} \\ m_{21} & m_{22} \end{bmatrix} K = \begin{bmatrix} k_{11} & k_{12} \\ k_{21} & k_{22} \end{bmatrix}$$

$$m_{11} = \int_{-a}^{a} m(x)\zeta^2 dx, m_{22} = \int_{-a}^{a} I_{xx}\rho^2 dx,$$

$$m_{12} = m_{21} = 0$$

$$k_{11} = -\int_{-a}^{a} m(x)\Omega^2\zeta^2 \,\mathrm{dx} - \int_{-a}^{a} gm(x)\left[\int_{0}^{x}(\zeta')^2 dz\right]dx + \tag{19}$$

$$+\int_{-a}^{a} EI_z(x)\zeta''^2 dx + \left(\mathrm{k}_{T_1} + k_{T_2}\right)\left(\zeta'|_{\mp a}\right)^2$$

$$k_{22} = \int_{-a}^{a} GJ_{xx}\rho'^2 dx, k_{12} = k_{21} = 0, Q_q^* = Q_q + Q_q^0$$

$$Q_q^0 = \int_{-a}^{a} m(x)\Omega^2 R\zeta dx$$

### 2.4 Modal Frequency

This section investigates the effects of variable blade length on the blade's natural frequencies. Thus, in the absence of gravity, aerodynamic forces, and torsional stiffness, the equations of motion (17-18) reduce to:

$$\begin{aligned} &\ddot{q}\int_{-a}^{a} m(x)\zeta^2 dx - q\int_{-a}^{a} m(x)\Omega^2\zeta^2 \,\mathrm{dx} \\ &-\int_{-a}^{a} m(x)\Omega^2 R\zeta dx + q\int_{-a}^{a} EI_z(x)\zeta''^2 dx = 0 \end{aligned} \tag{20}$$

$$\ddot{b}\int_{-a}^{a} I_{xx}\rho^2 dx + b\int_{-a}^{a} J_{xx}\rho'^2 dx = Q_b \tag{21}$$

where, for the first mode shapes, $\zeta(x)$ and $\rho(x)$ are approximated by $\cos(\frac{\pi x}{2a})$ as plotted in Fig. 3.

Moreover, proportional damping [26] will be introduced to reach the steady-state condition, as will be discussed later (where α and β are real positive constants). $\bar{M}$ and $K$ are the mass and stiffness matrices as defined in (20).

$$[C] = \alpha[\bar{M}] + \beta[K] \tag{22}$$

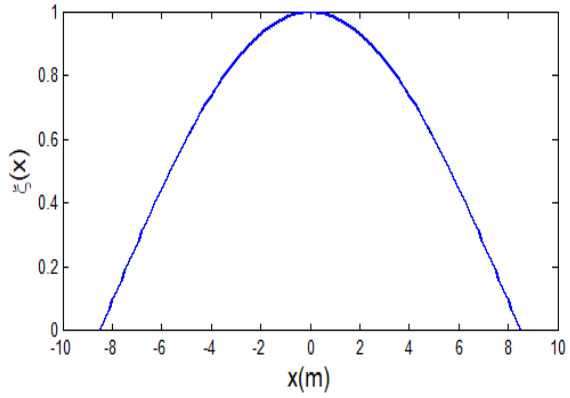


**Figure 3. Modal function along the span of the turbine**

## 3. AERODYNAMIC ANALYSIS

The main objective here is to evaluate the aerodynamic forces exerted by the fluid on the wind turbine blade. The two major forces are the normal and tangential forces, as illustrated below. As explained in the next section, Momentum theory is utilized in this regard considering the so-called double multiple streamtube models (DMST).

### 3.1 Double Multiple Streamtube Model (DMST)

The DMST model proposed by Paraschivoiu [27] merges the double actuator disk theory and the MST model to estimate the performance of Darrieus VAWT. As presented in Fig. 4, the calculation for the upwind and downwind zones is executed separately. Usually, the wind velocities in the upwind zone are higher than those in the downwind zone since the turbine blades will consume some energy to produce torque.

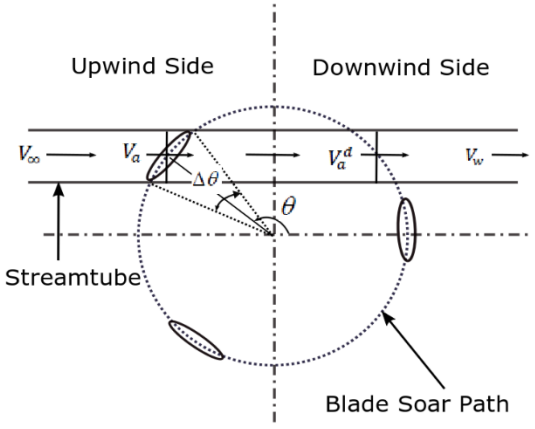


**Figure 4. Diagrammatic of DMST model**

To get the streamwise force at the actuator disk, the DMST model solves two equations simultaneously; the first equation originates from momentum conservation, and the second comes from the airfoil lift & drag coefficients and the local wind speed.

Upwind half $\frac{\pi}{2} \le \theta \le \frac{3\pi}{2}$

$$W = \sqrt{\left(V_a \sin\theta\right)^2 + \left(R\omega + V_a \cos\theta\right)^2} \tag{23}$$

$$\alpha = \tan^{-1}\left[\frac{(1-a)\cos\theta}{\lambda+(1-a)\sin\theta}\right] \quad (24)$$

Downwind half $-\frac{\pi}{2} \le \theta \le \frac{\pi}{2}$

$$W^d = \sqrt{\left(V_a^d \sin\theta\right)^2 + \left(R\omega + V_a^d \cos\theta\right)^2} \quad (25)$$

$$\alpha^d = \tan^{-1}\left[\frac{(1-a^d)\sin\theta}{\lambda+(1-a^d)\cos\theta}\right] \quad (26)$$

Once the new angle of attack and relative wind speed are determined using the new induction factor, the thrust coefficient, torque coefficient, and power coef–ficient can be determined. Equalizing the forces due to momentum conservations to those of blade element theory (more details are given in [28, 29]):

$$f_u(1-\mathrm{a}) = \pi a \quad (27)$$

where the upwind function $f_u$ is given by:

$$f_u = \frac{Nc}{8\pi R}\int_{\pi/2}^{3\pi/2}\left(C_n\frac{\cos\theta}{|\cos\theta|} - C_t\frac{\sin\theta}{|\sin\theta|}\right)\left(\frac{W}{V_a}\right)^2 d\theta \quad (28)$$

Thus, the power coefficient for the upwind half of the turbine is given by:

$$C_{P_u} = \frac{NcH}{2\pi A}\int_{\pi/2}^{3\pi/2} C_t\left(\frac{W}{V_\infty}\right)^2 d\theta \quad (29)$$

The downwind side of the turbines is treated the same way, and last, the power coefficients for the two half-cycles are added to obtain the overall power coefficient.

The overall normal and tangential forces are given by:

$$F_n = \frac{1}{2}C_n\rho cHW^2 \quad (30)$$

$$F_t = \frac{1}{2}C_t\rho cHW^2 \quad (31)$$

where the tangential force coefficient ($C_t$) is the resultant of the tangential components of lift and drag forces, and the normal force coefficient ($C_n$) is the resultant of the lift and drag normal components, which are given below for the case of zero pitch.

$$C_t = C_l\sin\alpha - C_d\cos\alpha \quad (32)$$

$$C_n = C_l\cos\alpha + C_d\sin\alpha \quad (33)$$

### 3.2 Tip Loss Consideration

The effect of the tip loss was considered while implementing the DMST model. Tip loss designates the propensity for losing the vorticity from any point on the wind turbine where the flow circulation changes, such as the blade's tip, thereby minimizing the efficacy of the blade and, consequently, the output power of the turbine [30]. Prandtl's tip loss factor is popularly utilized for VAWTs [28,31,32], which is given by:

$$F = \frac{2\arccos\left(e^{-\pi(\frac{H}{2}-|z|)/\mathrm{b}}\right)}{\pi} \quad (34)$$

where Z symbolizes the stream tube height away from the mid of the rotor (the equatorial position in the curved-blade rotor); the coefficient b is defined as follows in the upwind and downwind zones:

$$b = \frac{\pi V_e}{N\omega} = \frac{\pi V_\infty(1-2a)}{N\omega} \quad (35)$$

$$b^d = \frac{\pi V^d}{N\omega} = \frac{\pi V_e(1-2a^d)}{N\omega} \quad (36)$$

The angle of attack after correction, considering zero pitch, can be written as follows:

$$\alpha = \tan^{-1}\left[\frac{\mathrm{F}(1-a)\cos\theta}{\lambda+(1-a)\sin\theta}\right] \quad (37)$$

Consequently, the resultant velocity after correction read:

$$W = \sqrt{\left(FV_a\sin\theta\right)^2 + \left(R\omega + V_a\cos\theta\right)^2} \quad (38)$$

## 4. AEROELASTIC ANALYSIS

This section details the methodology cited in the aeroelastic analysis of VAWTs. The aeroelastic analysis is executed by coupling the structural dynamic equations studied earlier with the aerodynamic model, previously developed in section 3.

### 4.1 Aeroelastic Coupling

Methodically, in a fluid-structure interaction problem, the loose coupling between the two domains is performed by following two steps: first, the structural responses are evaluated due to the fluid loads, and then, the structural responses are used as feedback to the fluid domain. Here, these two steps are described in more detail [33].

#### 4.1.1 Structural Deflection

It was explained in the preceding headings how the tangential ($C_t$) and normal ($C_n$) force coefficients are obtained for each blade element. Note that these coefficients are calculated at the aerodynamic center (AC) located at the quarter chord of the blade (from the leading edge). It is worthwhile pointing out that the moment coefficient is assumed to be zero at AC. This assumption is particularly true for the high Reynolds number regime. Small aerodynamic moments exist at relatively smaller Reynolds numbers, which is assumed to be negligible in this analysis.

To apply the tangential and normal aerodynamic forces on the structure, these forces must be transformed to the elastic axis (EA) of the blade, which is located at the geometric center of the blade, as assumed before.

To perform this, a moment must be applied at EA, as illustrated in Fig. 5. The non-dimensional magnitude of

this moment is $C_m = C_n \frac{d^0}{b}$, where $\frac{d^0}{b}$ is the non-dimensional distance between EA and AC with respect to the half chord length b. The forces $F_t$ and $F_n$, are given by (31-32), whereas the moment is given by:

$$M = \frac{1}{2} C_m \rho b c H W^2 = F_n d_o \tag{39}$$

These forces are assumed to be evenly distributed over the aerodynamic blade element.

An accurate prediction of the structural vibration requires enough FEM elements. This number of FEM elements is typically greater than the ones needed for the aerodynamic model. Therefore, each aerodynamic blade element might constitute one to several FEM elements.

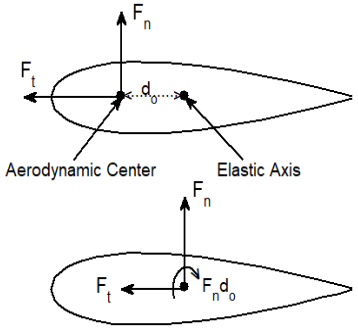


**Figure 5. Aerodynamic forces on the blade section**

#### 4.1.2 Aerodynamic Updates

After the structure's vibration, the aerodynamic loads must be modified to consider the structural deformation since the induced velocity, angle of attack, and radius will be updated due to the deformation and vibration-induced velocities, as detailed below.

$$\alpha = \tan^{-1}\left[\frac{\mathrm{F}(1-a+\frac{\dot{y}}{V_\infty})\cos\theta}{\lambda+(1-a)\sin\theta}\right]+\psi \tag{40}$$

$$r = R + y \tag{41}$$

$$W = \sqrt{\left(F(V_a+\dot{y})\sin\theta\right)^2+\left(R\omega+V_a\cos\theta\right)^2} \tag{42}$$

where $\psi$ is the angle of twist deformation and y is the transverse displacement. Thus, these new quantities are used to calculate the induced velocity and other vari–ables. It is worth mentioning that, since the DMST model is used here, the axial induction factor is a steady state parameter (calculated under steady-state condi–tions, which is the underlying assumption of momentum theory), and therefore, terms involving $\dot{y}$ are neglected in (41-43) which are only shown here for generality. This assumption may lead to the minimal effect of the structural deformations on the aerodynamics loads, as illustrated in the next section.

## 5. RESULTS AND DISCUSSION

This section evaluates the performance of the DOE/Sandia 17m turbine in terms of aerodynamic and structural performance with- and without aerodynamic loads. The aerodynamic loads were estimated using the DMST model, which is the best among the stream tube models. For the structural analysis, thin beam theory was utilized, and the SB-VAWT blade was modeled as a slender beam exposed to deformation of mainly bending and twisting, as detailed earlier. To simplify the analysis and facilitate the computation, one blade of the VAWT was investigated, which is considered one of the limitations of this study. In other words, the coupling between the blades is neglected, assuming that the wake of the blades is less significate at low wind speeds. Also, the deformation on the blades is expected to be similar, and modeling one blade will provide useful insights regarding the structural performance in general. In addition, more deformation of the turbine tower is expected since the centrifugal force is in one direction, unlike the multiple blades scenario where the centrifugal forces from different blades will balance each other, and low deflection on the tower is possible.

The second shortcoming of this work is the lack of a dynamic stall model in the aerodynamic part, which is the main reason for the discrepancy between the modeling results and experimental data at low tip speed ratios. However, it was shown in previous work [34] that using the DMST model with tip loss correction can only predict the aerodynamic loads with high accuracy. Moreover, as shown in Fig. 6, good performance is achieved without a dynamic stall model, which is recommended for future work.

### 5.1 Aerodynamic Performance

Inclusive, experimental data in the literature are obtainable for the curved-blade (Φ-type) VAWTs, yet, limited results have been reported about H-rotors (SB-VAWTs) [31,35]. Therefore, for performance assess–ment and testing using the DMST model, we selected the 17m diameter turbines tested at Sandia National Laboratories (SNL), having the properties in Table 1 [36], for comparison. The power coefficient against TSR is graphed in Fig.6 using the DMST model and compared with experimental and numerical results from the literature. The field data were taken from [6], and [37], and the numerical results of [38] were also included in the graph where an acceptable match among the results was achieved. The DMST model was programmed in Matlab script, beginning with a few stream tubes at first and refining gradually to see if the performance is enhanced. It turned out that using 29 stream tubes was enough and led to acceptable results.

**Table 1. Dimensions of Sandia 17m turbine [36]**

| | |
|---|---|
| Number of Blades | 2 |
| Radius (m) | 8.5 |
| Chord (m) | 0.61 |
| Blade Length (m) | 17.34 |
| Aerofoils | NACA0015 |

In Fig. 7, the aerodynamic torque of the turbine is given as a function of the blade azimuth position and compared with torque measurements of the Sandia 17m turbine [39] and other numerical results. As shown in

Fig. 7 (a), there is some mismatch between the results, which is attributed to the dynamic stall phenomenon, since at low TSRs, due to the smaller value of the blade velocity, the relative velocity makes a larger angle with the blade velocity.

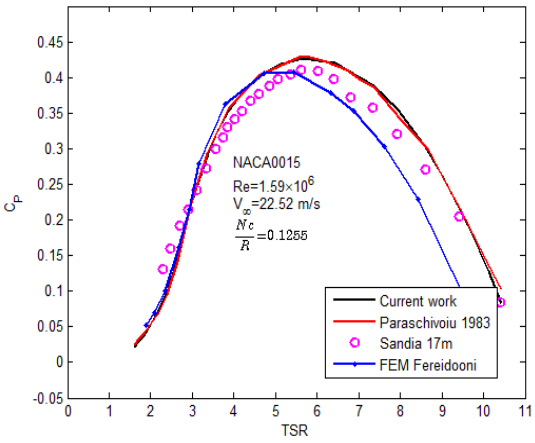


**Figure 6. The power coefficient versus TSR for DOE/Sandia 17m turbine at 50.6 rpm**

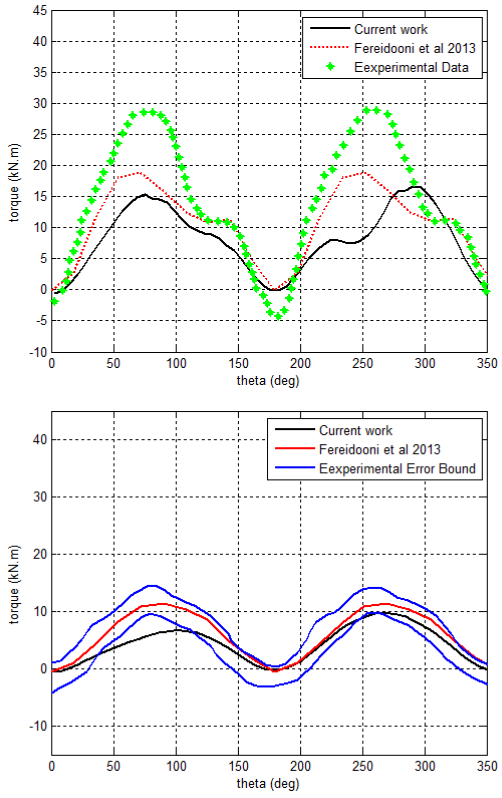


**Figure 7. Comparison of the torque generated by Sandia 17m turbine at 50.6 rpm, (a) TSR = 2.8, wind speed 16m/s (b) TSR = 4.36, wind speed 10.3m/s with Fereidooni [33] and experimental data of [39]**

Hence, the angle of attack becomes higher than the static stall angle. Consequently, the blade occasionally changes between stalled and un-stalled conditions, which reduces the torque generated. On the other hand, at higher TSRs (4.36 in Fig. 7 (b)), the angle of attack varies within a range smaller than the static stall angle, and thus, the dynamic stall pheno–menon is not critical, as discussed in [6,40]. Furthermore, in Fig. 7 (b), there is some discrepancy between the predicted torque using the DMST model and other results at an azimuth position of 50-100 deg, which is related to the fact that a straight-bladed turbine is investigated here while the other results were obtained for the troposkein shaped VAWT, and hence some discrepancy is expected.

### 5.2 Structural Performance without Aerodynamic Loads

The equations of motions derived in section II were solved and simulated in a Matlab environment. However, before presenting the results, the material properties and specifications of the turbine are given in Tables 2 and 3. It is worth mentioning that DOE/Sandia 17 m turbine was originally constructed using NACA0012 blades made of Fiberglass/ Honeycomb /Aluminum Extrusion, having a chord length of 21 in. However, another version using NACA0015 blades made of Aluminum extrusion, having a chord length of 24 in, was also introduced [36,41,42].

**Table 2. Material properties of the selected Aluminium alloy**

| Property | Value |
|---|---|
| Density | 2700 kg/m$^3$ |
| Young's Modulus | 70 GPa |
| Shear Modulus | 26 GPa |

**Table 3. Specifications of Sandia 17m turbine [14], [15]**

| | |
|---|---|
| Blade | NACA0015 |
| Material | Extruded Aluminum |
| Radius | 6 m |
| Cross-sectional weight | 15.09 kg/m |
| The second moment of the area around chord line ($I_z$) | $8.59\times10^{-6}\,m^4$ |
| The second moment of the area around centroid ($J_x$) | $1.37\times10^{-4}\,m^4$ |
| Mass moment of inertia around the blade cross-section about the centroid per unit length ($I_x$) | 0.37 kg. m |

#### 5.2.1 Modal Frequency

The estimated modal frequencies for twist and bend for a reference case of a parked rotor ($\Omega = 0$) are displayed in Fig.8 as a function of the blade half-length, $a$. The torsional frequency is greater than that of the transverse bending, indicating that the torsional stiffness is greater than the bending stiffness, and more deformation in the bending side is expected.

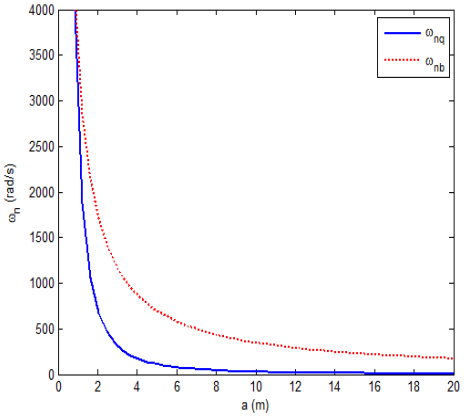


**Figure 8 variation of $\omega_{nq}$ and $\omega_{nb}$ with half-length "a" when Ω = 0**

### 5.2.2 Structural Displacement due to Centrifugal Forces Only

The following results for transverse and rotational displacements of the elastic axis of the blade at the middle of the rotor are obtained by solving the system (21-22) by letting $Q_q = Q_b = 0$ which means the aerodynamic forces are not included. $C = 8\times10^{-1}M + 5\times10^{-3}K$. These values were selected based on [26] as a guide with some trail and error to bring the response to steady-state conditions. It is worth pointing out that, to reach a steady-state condition, a proportion damping was introduced, as mentioned earlier (22).

As shown in Fig. 9 (a), there is some oscillation at the beginning until a steady state value of 156 cm is reached for the transverse displacement, which is directly related to the centrifugal force $Q_{q0} = \int_{-a}^{a} m(x)\Omega^2 R\zeta\, dx$, which is constant at the middle of the blade (at the equator in the corresponding curved blade turbine) as shown in Fig.10 (a). It could be demonstrated that the transverse displacement will totally disappear when the centrifugal force is zero. On the other hand, there is no twist deformation as depicted in Fig. 9 (b), which is expected since there is no forcing term in the twist equation, as visualized in Fig. 10 (b). Once a forcing term is included (like the aerodynamic force), twisting will occur, as we will see in the upcoming headings.

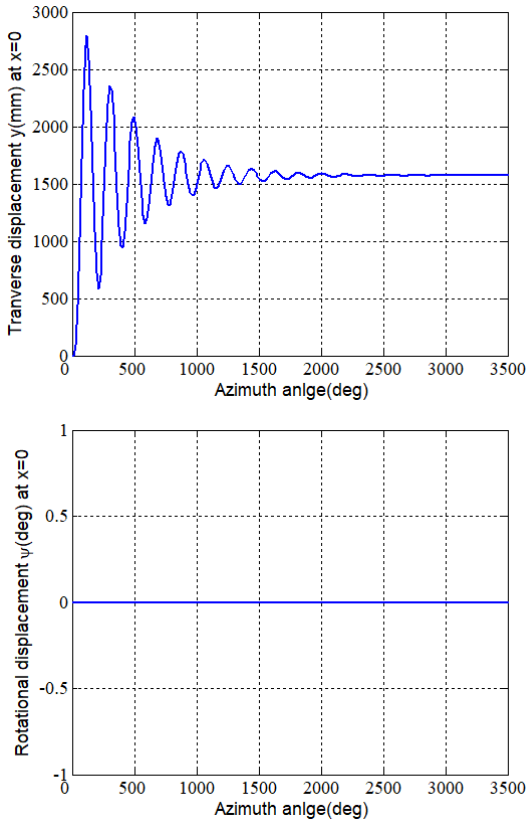


**Figure 9. Displacement at the middle of the elastic axis (a) Transverse and (b) Rotational displacement, for a = 8.5m, Ω=3.8750 rad/s (due to centrifugal forces only)**

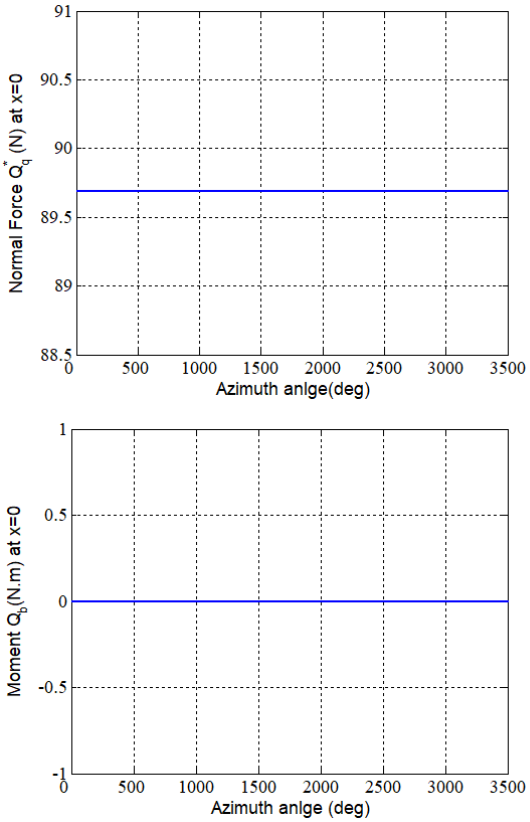


**Figure 10. Forces at the middle of the elastic axis: (a) Nor–mal force and (b) twisting moment about the elastic axis, for a = 8.5m, Ω=3.8750 rad/s (due to centrifugal forces only)**

### 5.3 Structural Displacement due to Aerodynamic Forces Only

Here the centrifugal forces are not included; only the aerodynamic forces are considered. As indicated in Fig. 11 (a), the transverse displacement has significantly reduced due to the absence of the centrifugal force, which is much greater than the aerodynamic force. Moreover, as depicted (Fig. 11 (b)), the twist angle fluctuates between 1.5 and -1.5 degrees with a constant amplitude, implying that the damping has negligible/no effect on the rotational displacement. It is noticeable that both displacements are oscillating with constant amplitude, likewise the corresponding forcing terms as provided in Fig. 12 (a-b). It is clear from that figure that the moment about the elastic axis of the blade is much smaller than the normal force (in the radial direction), which is why the translational displacement is much greater than the rotational displacement.

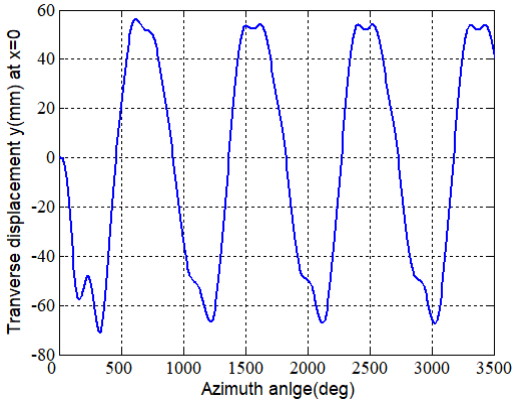

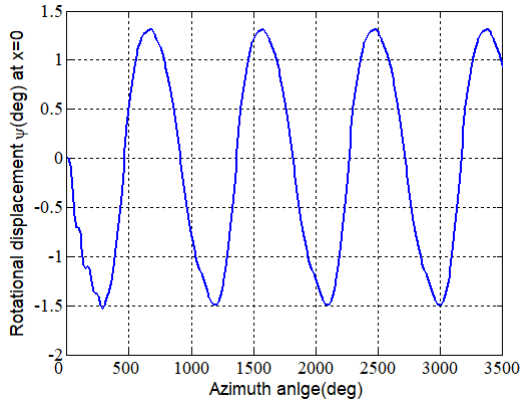


**Figure 11 Displacement at the middle of the elastic axis (a) Transverse and (b) Rotational displacement, for a = 8.5m, Ω=3.8750 rad/s (due to aerodynamic forces only)**

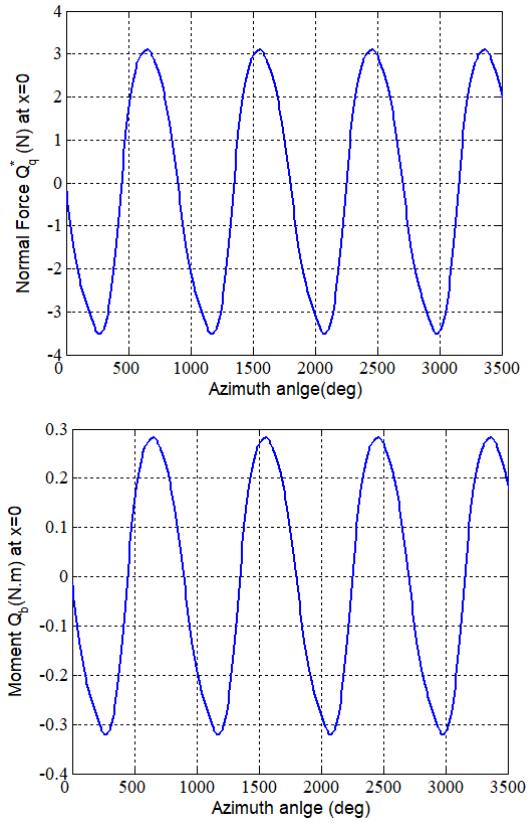


**Figure 12. Forces at the middle of the elastic axis: (a) Normal force and (b) twisting moment about the elastic axis, for a = 8.5m, Ω=3.8750 rad/s (due to aerodynamic forces only)**

### 5.4 Structural Displacement due to Aerodynamic and Centrifugal Forces

Figure 13 presents the transverse displacement (a) and the rotational displacement (b) of the elastic axis of the blade. As displayed, the twist angle fluctuates with constant amplitude as before (unchanged) since it does not depend on the centrifugal force. The steady-state value of the translation displacement is also experiencing some damping which is attributed to the cyclic nature of the aerodynamic forces, which are linearly dependent on transverse and twisting directions.

The mean value of translational displacement is 156 cm, which is much greater than that of a curved blade machine (troposkein shape); in [33], a mean value of 25mm was reported. This high deformation of the SB-VAWT blade is attributed to the fact that straight-bladed machines usually generate higher bending moments and thus more deformation [38]. Moreover, compared to SB-VAWTs, the centrifugal force has a little effect on curved blade machines since they already have the shape that centrifugal force is trying to make. Though they have higher deformation, SB-VAWTs permit the size of the rotor to be reduced to a reasonable value for a specified performance. It was found in previous work [34], that starting from an aspect ratio of around one and reducing the diameter of the SB-VAWT significantly improve the performance and enhance the peak power, emphasizing the suitability of straight blade turbines for small rotor sizes and low wind situations. Finally, the geometric simplicity and low manufacturing cost may compensate for the high bending moments issue [38, 43].

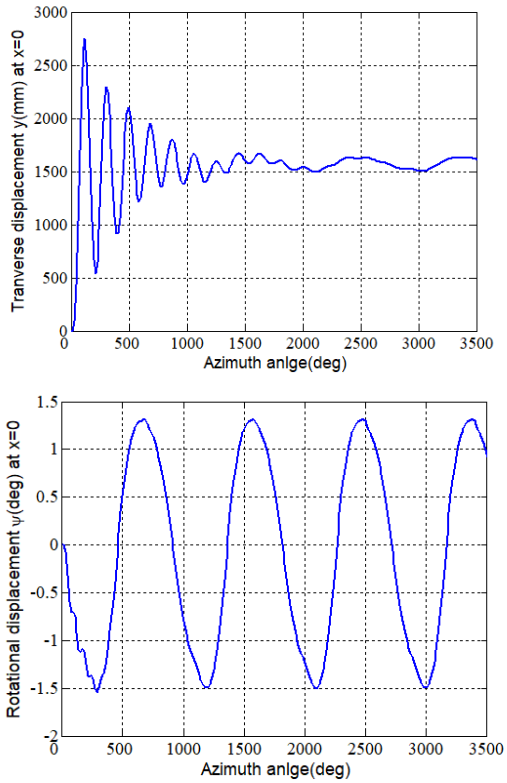


**Figure 13. Displacement at the middle of the elastic axis (a) Transverse and (b) Rotational displacement, for a = 8.5m, Ω=3.8750 rad/s (due to centrifugal & aerodynamic forces)**

The radial force and twisting moment about the elastic axis at the middle of the rotor are provided in Fig. 14. Since it is pure aerodynamic, the twisting mo–ment is unchanged, as shown in Fig. 14 (b). On the other hand, the normal force oscillates with an average value of around 89.6 N, which is the same as the con–stant value reported in Fig. 10 (a) (the case of cen–trifugal force only). This highlights that the aerody–namic loads are cyclic and thus introduce the transient response part of the total force acting on the blade.

### 5.5 Comparison of different loading cases in one graph

Figure 15 compares the three cases (aerodynamic loads only, centrifugal forces only, and both). It is evident that, from Fig. 15 (a), the transverse displacement is

mainly dominated by the centrifugal forces to the extent that the aerodynamic forces' effect is minimal. This is attributed to the fact that; the aerodynamic force magnitude is relatively small compared with centrifugal force, as displayed in Fig. 16 (a). The effect of the aerodynamic forces only appears in terms of oscillation due to the cyclic nature of these forces.

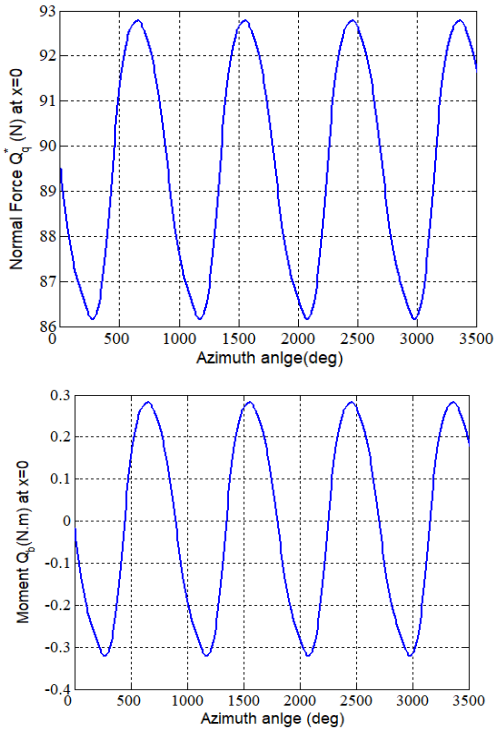


**Figure 14. Forces at the middle of the elastic axis: (a) Normal force and (b) and twisting moment about the elastic axis, for a = 8.5m, Ω=3.8750 rad/s (due to centrifugal & aerodynamic forces)**

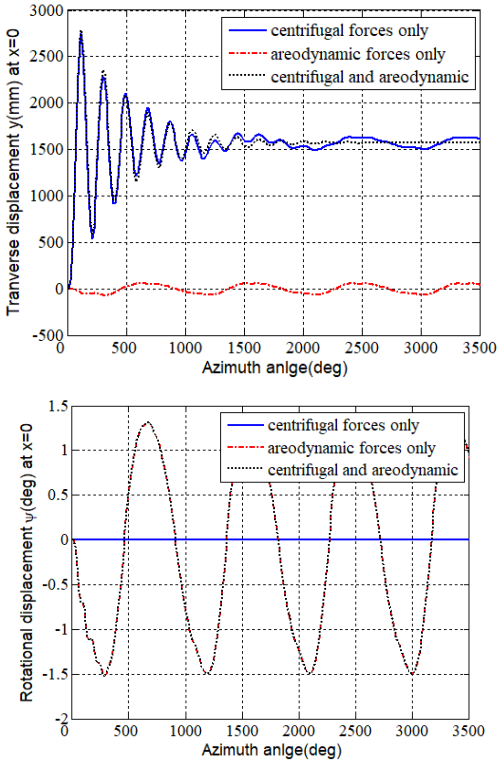


**Figure 15. Displacement at the middle of the elastic axis (a) Transverse and (b) Rotational displacement, for a = 8.5m, Ω=3.8750 rad/s (comparison of different loading cases)**

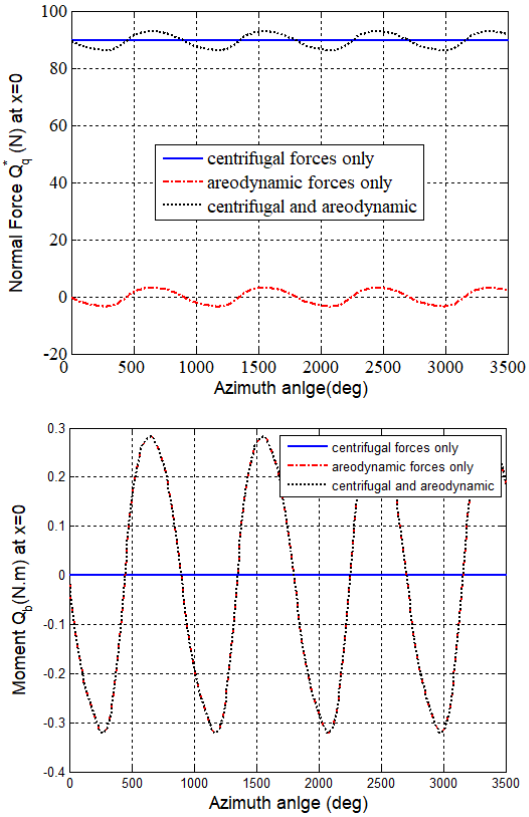


**Figure 16. Forces at the middle of the elastic axis: (a) Nor–mal force and (b) and twisting moment about the elastic axis, for a = 8.5m, Ω=3.8750 rad/s (comparison of different loading cases)**

On the other hand, the moment about the elastic axis and the corresponding rotational displacement is only caused by the aerodynamic forces, as shown in Fig. 16 (b), and independent of the centrifugal forces since the system's dynamics are uncoupled, as explained earlier.

## 6. CONCLUSION

The dynamic response of the SB-VAWT blade has been investigated using a linearized model of the system based on reduced order modeling considering one assu–med mode for bend and twist. The structural perfor–mance has been investigated considering the centrifugal and/or aerodynamic forces. The double multiple stream tube model was utilized for the aerodynamic force estimation. The equations of motion were solved nume–rically using the average acceleration method technique for time integration. The obtained results were compared with experimental and numerical data for DOE/Sandia 17 turbine available in the literature.

For the case of aerodynamic forces only, the trans–verse and rotational displacements are oscillating within 70mm and 1.5 deg, respectively, which is directly related to the cyclic aerodynamic forces causing them. This cyclic loading also is the reason for the lasting oscillation in the transverse direction even in the presence of damping, in the case of combined loads (aerodynamic + centrifugal). Moreover, the centrifugal force makes a considerable deformation in the crosswise direction with no effect on the twisting side.

The transverse displacement has a steady state (mean) value of 156 cm. In addition, it is observable

that the structural displacement has little effect on the aerodynamic loads, which is attributed to the fact that the axial induction factor used in the DMST model is calculated under steady-state conditions, hence limiting the effect of the transient response caused by the structural deformations. Finally, the blade of SB-VAWT experiences higher deformation and bending stresses compared to the curved blade machines. This can be further investigated by evaluating the fatigue life of the blade of SB-VAWT and comparing it with that of curved blade machines, which is recommended for future work.

## ACKNOWLEDGMENT

The authors are grateful for the support of their funding body represented by the Deanship of Scientific Research (DSR) at King Fahd University of Petroleum and Minerals (KFUPM) through the National Science, Technology and Innovation Plan (NSTIP) of the King Abdulaziz City for Science and Technology (KACST): Grant Number 14-ENE2337-04. Besides, the first author cheers the aid supplied by KFUPM Endowment via Mr. Luhaidan Scholarship Program.

## REFERENCES

[1] E. Verkinderen, B. Imam, 'A simplified dynamic model for mast design of H-Darrieus vertical axis wind turbines (VAWTs)', *Engineering Structures*, vol. 100, pp. 564–576, 2015.

[2] N. Natarajan, S. Rehman, N. S. Shiva, and M. Vasudevan, 'Evaluation of wind energy potential of the state of Tamil Nadu, India based on trend analysis', *FME Transactions*, vol. 49, no. 1, pp. 244–251, 2021.

[3] M. Bashaer, O. I. Abdullah, and A. I. Al-Tmimi, 'Investigation and analysis of wind turbines optimal locations and performance in Iraq', *FME Transactions*, vol. 48, no. 1, pp. 155–163, 2020.

[4] K. R. V. Kaza and R. G. Kvaternik, 'Aeroelastic equations of motion of a Darrieus vertical-axis wind-turbine blade', 1979.

[5] F. Nitzsche, 'Aeroelastic analysis of a Darrieus type wind turbine blade with troposkien geometry', 1983.

[6] A. Fereidooni, 'Numerical study of aeroelastic behaviour of a troposkien shape vertical axis wind turbine', Carleton University, 2013.

[7] M. S. Hameed and S. K. Afaq, 'Design and analysis of a straight bladed vertical axis wind turbine blade using analytical and numerical techniques', *Ocean Engineering*, vol. 57, pp. 248–255, 2013.

[8] B. A. Al-Bakri and R. M. Aljuhashy, 'The aerodynamics of the wavy blade under the effect of fluctuated wind flow', *FME Transactions*, vol. 49, no. 3, pp. 704–710, 2021.

[9] B. Rašuo, M. Dinulović, A. Veg, A. Grbović, and A. Bengin, 'Harmonization of new wind turbine rotor blades development process: A review', *Renewable and Sustainable Energy Reviews*, vol. 39, pp. 874–882, 2014.

[10] B. P. Rašuo and A. Č. Bengin, 'Optimization of wind farm layout', *FME transactions*, vol. 38, no. 3, pp. 107–114, 2010.

[11] J. Svorcan, Z. Trivković, T. Ivanov, M. Baltić, and O. Peković, 'Multi-objective constrained optimizations of VAWT composite blades based on FEM and PSO', *FME Transactions*, vol. 47, no. 4, pp. 887–893, 2019.

[12] T. D. Ivanov, A. M. Simonović, J. S. Svorcan, and O. M. Peković, 'VAWT optimization using genetic algorithm and CST airfoil parameterization', *FME Transactions*, vol. 45, no. 1, pp. 26–31, 2017.

[13] O. Kapucu, *Vibrational analysis of vertical axis wind turbine blades*. Michigan State University, 2014.

[14] F. Afzali, O. Kapucu, and B. F. Feeny, 'Vibration analysis of vertical-axis wind-turbine blades', in *ASME 2016 International Design Engineering Technical Conferences and Computers and Information in Engineering Conference*, 2016, p. V008T10A047-V008T10A047.

[15] A. F. A. hakeem Saleh, *Modal analysis of vertical-axis darrieus wind turbine blade with a troposkein shape*. Michigan State University. Mechanical Engineering, 2017.

[16] A. Saleh and B. F. Feeny, 'Modal analysis of a vertical-axis darrieus wind turbine blade with a troposkein shape', in *Topics in modal analysis & testing, volume 9*, Springer, 2019, pp. 325–327.

[17] S. Rehman, S. A. Khan, and L. M. Alhems, 'The effect of acceleration coefficients in Particle Swarm Optimization algorithm with application to wind farm layout design', *FME Transactions*, vol. 48, no. 4, pp. 922–930, 2020.

[18] M. Dinulović, B. Rašuo, M. R. Trninić, and V. M. Adžić, 'Numerical modeling of Nomex honeycomb core composite plates at meso scale level', *FME Transactions*, vol. 48, no. 4, pp. 874–881, 2020.

[19] B. Hand and A. Cashman, 'A review on the historical development of the lift-type vertical axis wind turbine: From onshore to offshore floating application', *Sustainable Energy Technologies and Assessments*, vol. 38, p. 100646, 2020.

[20] E. E. Meyer and C. E. Smith, 'Aeroelastic Analysis of the Darrieus Wind Turbine', *Journal of energy*, vol. 7, no. 6, pp. 491–497, 1983.

[21] E. A. Khazem, O. I. Abdullah, and L. A. Sabri, 'Steady-state and vibration analysis of a WindPACT 1.5-MW turbine blade', *FME Transactions*, vol. 47, no. 1, pp. 195–201, 2019.

[22] S. H. Kumar, R. Anand, 'A case study on damage detection of wind turbine composite blade', *FME Transactions*, vol. 47, no. 1, pp. 135–141, 2019.

[23] T. A. Ismaeel, S. Aljabair, O. A. Abdulrazzaq, and Y. A. Abood, 'Energy recovery of moving vehicles' wakes in highways by vertical axis wind turbines', *FME Transactions*, vol. 48, no. 3, pp. 557–565, 2020.

[24] S. S. Rao, *Vibration of continuous systems*, vol. 464. Wiley Online Library, 2007.

[25] R. R. Craig and A. J. Kurdila, *Fundamentals of structural dynamics*. John Wiley & Sons, 2006.

[26] A. Ghorbel, O. Graja, T. Hentati, M. Abdennadher, L. Walha, and M. Haddar, 'The effect of the brake location and gear defects on the dynamic behavior of a wind turbine', *Arabian Journal for Science and Engineering*, pp. 1–13, 2020.

[27] I. Paraschivoiu, 'Double-multiple streamtube model for Darrieus in turbines', 1981.
[28] I. Paraschivoiu, *Wind turbine design: with emphasis on Darrieus concept*. Presses inter Polytechnique, 2002.
[29] A. A. Mohammed, H. M. Ouakad, A. Z. Sahin, and H. M. Bahaidarah, 'Vertical Axis Wind Turbine Aerodynamics: Summary and Review of Momentum Models', *Journal of Energy Resources Technology*, vol. 141, no. 5, p. 050801, 2019.
[30] A. Naseem *et al.*, 'Effect of vortices on power output of vertical axis wind turbine (VAWT)', *Sustainable Energy Technologies and Assessments*, vol. 37, p. 100586, 2020.
[31] Z. Zhao *et al.*, 'Study on variable pitch strategy in H-type wind turbine considering effect of small angle of attack', *Journal of Renewable and Sustainable Energy*, vol. 9, no. 5, p. 053302, 2017.
[32] C. E. Soraghan, W. E. Leithead, J. Feuchtwang, and H. Yue, 'Double multiple streamtube model for variable pitch vertical axis wind turbines', in *31st AIAA Applied Aerodynamics Conference*, 2013, p. 2802.
[33] A. Fereidooni, 'Numerical Study of Aeroelastic Behaviour of a Troposkien Shape Vertical Axis Wind Turbine', Carleton University, 2013.
[34] A. A. Mohammed, et al.,'Parametric study and comparison of aerodynamics momentum-based models for straight-bladed vertical axis wind turbines', *Arabian Journal for Science and Engineering*, pp. 1–13, 2019.
[35] A. A. Mohammed, A. Z. Sahin, and H. M. Ouakad, 'Numerical investigation of a vertical axis wind turbine performance characterization using new variable pitch control scheme', *Journal of Energy Resources Technology*, vol. 142, no. 3, 2020.
[36] M. H. Worstell, *Aerodynamic performance of the 17-metre-diameter Darrieus wind turbine*. Department of Energy, Sandia Laboratories, 1979.
[37] R. Wilson and S. Walker, 'Fixed wake theory for vertical axis wind turbines', 1983.
[38] I. Paraschivoiu and F. Delclaux, 'Double multiple streamtube model with recent improvements.', *J. ENERGY.*, vol. 7, no. 3, pp. 250–255, 1983.
[39] G. M. McNerney, 'Accelerometer measurements of aerodynamic torque on the DOE/Sandia 17-m vertical axis wind turbine', *NASA STI/Recon Technical Report N*, vol. 81, 1981.
[40] D. Berg, 'Recent improvements to the VDART3 VAWT code', Sandia National Labs., Albuquerque, NM (USA), 1983.
[41] S. F. Johnston Jr, 'Proceedings of the vertical axis wind turbine (VAWT) design technology seminar for industry', Sandia Labs., Albuquerque, NM (USA), 1980.
[42] M. Worstell, 'Measured aerodynamic and system performance of the 17-m research machine', *VAWT*, pp. 233–258, 1980.
[43] A. Korobenko, M.-C. Hsu, I. Akkerman, and Y. Bazilevs, 'Aerodynamic simulation of vertical-axis wind turbines', *Journal of Applied Mechanics*, vol. 81, no. 2, 2014.

**NOMENCLATURE**

| | |
|---|---|
| $C_P$ | Power Coefficient |
| $M$ | Aerodynamic torque, N.m |
| $\bar{M}$ | Mass matrix |
| $K$ | Stiffness matrix |
| $N$ | Number of blades |
| $c$ | Chord length of the blade, m |
| $R, D$ | Radius/diameter of the wind turbine, m |
| $H$ | Hight of the blade/turbine, m |
| $a$ | Half-length of the blade |
| $\sigma$ | Solidity ( $\sigma = Nc / R$ ) |
| $\lambda$ | Tip speed ratio (TSR), $\lambda = \frac{\omega R}{V_\infty}$ |
| $\omega, \Omega$ | Rotor angular velocity, rad/s (RPM) |
| $V_a, V_a^d$ | Upstream/Downstream induced velocity, m/s |
| $V_\infty$ | Free stream velocity, m/s |
| $W, \mathrm{W}^d$ | Relative velocity upstream/ downstream, m/s |
| $V_c, V_n$ | Chordal/Normal velocity component, m/s |
| $\theta$ | Azimuth angle |
| $\alpha, \alpha^d$ | Upstream/Downstream angle of attach |
| $C_l, C_d$ | Airfoil left/ drag coefficient |
| $C_t, C_n$ | Tangential/ Normal coefficient |
| $\rho$ | Density, Modal function |
| $A$ | Rotor/turbine swept area, $m^2$, $(A = 2HR)$ |
| $a, a^d$ | Upwind and downwind induction factors |
| $f_u, f_d$ | Upwind and downwind functions |
| $F_t, F_n$ | Normal and tangential force, N |
| $y$ | Transverse displacement (m) |
| $s$ | Foreshortening term (m) |
| $q(t), b(t)$ | Modal coordinates |
| $T, V$ | Kinetic/potential energy |
| $d_o$ | Distance between EA and AC |

***Acronym***

| | |
|---|---|
| VAWT | Vertical Axis Wind Turbine |
| SB-VAWT | Straight-Bladed Vertical Axis Wind Turbine |
| DMST | Double Multiple Streamtube |
| DOE | Department of Energy (US) |
| EA | Elastic Axis |
| AC | Aerodynamic Centre |
| FEM | Finite Element Method |
| FEA | Finite Element Analysis |

## АЕРОЕЛАСТИЧНА АНАЛИЗА ЛОПАТИЦЕ ВЕТРОТУРБИНЕ СА РАВНИМ ЛОПАТИЦАМА ВЕРТИКАЛНЕ ОСЕ

**А.А.М. Фадлала, А.З. Сахин, Х.М. Оуакад, Х. Бахаидарах**

Да би се спречиле појаве треперења у турбини на ветар, минимизирале вибрације и продужиле животни век лопатица, потребна је систематска анализа да би се истражили ефекти између цикличних аеродинамичких оптерећења и струк–турних перформанси турбине. У овом раду се истражује динамичка анализа лопатице ветротур–бине са вертикалном осовином (СБ-ВАВТ) са равним лопатицама и уведен је поједностављени приступ енергетским једначинама Ојлерове греде подвргнуте увијању и попречном савијању. Аеродинамичка оптерећења су процењена кориш–ћењем модела цеви са двоструким вишеструким током. Они се уводе у динамички модел у аероеластичном споју, где се структурни помаци враћају да би се ажурирала аеродинамичка оптере–ћења коришћењем методе просечног убрзања за нумеричку интеграцију једначина. Моделирање редукованог реда се тада намеће на основу првих модова вибрација. Утврђено је да структурно померање има мали утицај на аеродинамичка оптерећења, а СБ-ВАВТ имају веће попречне пома–ке у поређењу са онима код ВАВТ са закривљеним лопатицама.